Experimental Study of Adhesively Bonded Single Lap Joint Behaviour in CFRP-to-CFRP, Al-to-Al, and CFRP-to-Al Configurations

Kosim Abdurohman[1,*], Taufiq Satrio Nurtiasto[1], Rezky Agung Pratomo[2], Nur Mufidatul Ula[1], Afid Nugroho[1], Awang Rahmadi Nuranto[1], Riki Ardiansyah[1], Ryan Hidayat[3], Rian Suari Aritonang[1], Fajar Ari Wandono[1]

[1]Research Centre for Aeronautics Technology, National Research and Innovation Agency, Bogor, Jawa Barat 16350, Indonesia
[2]Department of Metallurgy and Material Engineering, Faculty of Engineering, University of Indonesia, Depok, Jawa Barat 16424, Indonesia
[3]Department of Mechanical Engineering, Faculty of Engineering, University of Indonesia, Depok, Jawa Barat 16424,Indonesia

*Author to whom correspondence should be addressed:
Email: kosi001@brin.go.id

(Received December 24, 2024; Revised September 12, 2025; Accepted September 27, 2025)

Abstract: This study evaluates the tensile performance of single-lap joints with three configurations: CFRP-to-CFRP, Al-to-Al, and CFRP-to-Al. The effect of CFRP and aluminum adherends on joint strength was analyzed based on surface characteristics and mechanical properties. CFRP substrates were fabricated using vacuum-assisted resin infusion with vinyl ester resin and unidirectional carbon fibers, while aluminum plates were cut to ASTM D5868 standards. Epoxy adhesive was employed, and surface preparation included 800-grit sanding to enhance bond quality. Surface roughness, wettability, and morphology were characterized using a surface roughness tester, contact angle, and atomic force microscopy measurements. Sanding significantly reduced surface roughness (Ra) for CFRP from 6.48 ± 0.24 μm to 1.49 ± 0.19 μm, improving surface wettability. Aluminum exhibited lower contact angles than CFRP, reflecting its distinct surface properties. Tensile tests of the epoxy adhesive revealed an ultimate tensile strength of 54.30 ± 2.20 MPa and a tensile modulus of 2.21 ± 0.08 GPa, confirming its suitability for SLJs. Lap shear tests demonstrated that CFRP-to-CFRP joints achieved the highest average shear strength (5.05 ± 0.64 MPa), followed by Al-to-Al (3.03 ± 0.57 MPa) and CFRP-to-Al (3.52 ± 0.75 MPa). The CFRP-to-Al configuration exhibited the highest variability due to material incompatibilities. Failure analysis indicated mixed adhesive and cohesive failure modes across all configurations, with CFRP-to-CFRP joints showing superior bond consistency. These findings highlight the critical role of material compatibility and surface treatment in optimizing SLJ performance for composite and dissimilar material joints.

Keywords: CFRP; composite-to-composite joints; composite-to-metal joints; epoxy adhesive; metal-to-metal joints; single lap bonded joints

1. Introduction

The rapid expansion of the fabrication sector necessitates the development of sustainable materials with excellent properties, among which composites have emerged as a promising solution for diverse applications[1)]. Composites, known for their high specific strength, stiffness, and failure strain, are widely used in lightweight structures like airplanes and automobiles, with fiber-reinforced polymers increasingly replacing stainless steel in aerospace due to their low thermal expansion, superior corrosion resistance, and excellent damping properties[2–7)]. The growing use of composites in industries such as wind energy, military, marine, automotive, civil engineering, and sports has driven increased interest in reliable joining techniques for composite components[2,6)]. However, the use of composites

Cite: K. Abdurohman et al., "Experimental Study of Adhesively Bonded Single Lap Joint Behaviour in CFRP-to-CFRP, Al-to-Al, and CFRP-to-Al Configurations". Evergreen, 12 (03) 1531-1544 (2025). https://doi.org/10.5109/7388847.

is limited by their low fracture toughness and high moisture absorption[8].

Joints are classified into mechanical and adhesive types, with mechanical joints relying on rivets or bolts and adhesive joints using an interlayer of adhesive between adherends. Adhesive joints are preferred for composites due to their superior fatigue resistance, lightweight contribution, ability to distribute loads over larger areas, and the absence of perforations or holes. Adhesive joints are challenging to disassemble for inspection or repair, require precise surface preparation, and are influenced by service conditions[9]. The adhesive joining of various materials, especially metals and composites, opens up new opportunities in contemporary structural design. Within this scope, the single lap joint (SLJ) is a basic yet effective bonding method, gaining considerable attention in research for its simplicity and efficiency[10].

Adhesively bonded joints are more sophisticated than mechanical ones and are significantly influenced by environmental factors such as temperature and humidity. Additionally, achieving a reliable bond requires precise surface preparation and geometric accuracy during the manufacturing process[11]. Adhesive bonding of long sections or thin composites requires more precise and thorough surface treatment[12].

Mechanical treatments like grit blasting or sanding improve surface roughness to enhance mechanical interlocking, with manual sanding commonly employed in composite joint studies. Zaldivar et al. prepared the surface of the carbon composite by hand-sanding with sandpapers of various grit sizes[13]. Bautista et al.[14], Purnomo et al.[15], Zhang et al.[16], Huang et al.[17], Choudhury and Debnath[18], Hu et al. [19], Freitas and Sinke[20], Akpinar et al.[21], and Sun et al.[22] treated the specimen surface by sanding followed by cleaning with acetone prior to bonding. Sugiman et al. prepared the specimen surfaces by treating them with hydrochloric acid followed by abrasion with sandpaper[23]. Various investigations have compared surface treatments like sanding, grit blasting, CO2 laser irradiation, and combinations such as sanding-grit blasting-peel ply, including the impact of sandpaper grit size on composite joints[24–27].

Adhesive bonded joints consist of substrates, a bonding layer, and the substrate-adhesive interface, where enhancing the interface can significantly improve joint strength[28,29]. Surface characteristics, including surface-free energy, topography, and substrate hardness, strongly influence substrate-adhesive interfaces, with surface-free energy being crucial for adhesion, adsorption, and wettability[30]. The theory of mechanical interlocking suggests that cured adhesive produces a mesh-like bond by filling gaps in the substrate's irregular surface[31]. Surface roughness significantly influences mechanical interlocking, thereby enhancing bonding strength[32].

Mechanical surface treatment using sandpaper is a straightforward and effective method to achieve adequate surface quality. Dehaghani et al. demonstrated that sandpaper surface treatment produces higher joint strength than grit blasting, offering adjustable surface roughness and texture based on sandpaper grit size while allowing control over sanding direction[24]. The surface roughness and texture achieved through sandpaper treatment depend on grit size and sanding direction, yet limited research has focused on how these factors influence the adhesive performance of composite joints[27]. Boutar et al. demonstrated that reduced surface roughness and improved wettability enhance the SLJ strength of aluminum. However, as carbon fiber laminates are anisotropic and differ significantly from aluminum, these findings serve as a reference but may not fully apply to laminated composites[33].

Numerous studies have explored the bonding mechanisms of composite-to-metals bonded joints. Ramaswamy et al. investigated the influence of load eccentricity angle and adhesive spew geometry on the bonded SLJ involving carbon-fiber thermoplastic composites and Al-Mg alloy adherends[34]. Grefe et al. examined the impact of fiber orientation on the shear strength and fracture behavior of bonded SLJ between CFRP and cold-rolled mild steel[35]. De Freitas et al. evaluated the impact of salt spray conditions on the performance of CFRP and carbon steel joints through peel tests[36]. Ramaswamy et al. also evaluated the influence of grit blasting as a surface pre-treatment on the joint performance of carbon-fiber thermoplastic prepreg composites and Al-Mg alloys under static and dynamic loading conditions[37]. Pitta et al. investigated the repair of aircraft lap joints using CFRE laminates with fibers in a satin weave configuration and AA 2024-T3 under static loading conditions[38]. Sugiman et al. investigated the impact of environmental media and aging conditions on the residual strength of GFRP-to-steel bonded joints[23]. The influence of overlap length and adhesive thickness on the static and fatigue strength of CFRP-AA 7050-T6 single lap joints (SLJs) was examined. Longer overlap lengths and thicker adhesives were found to reduce fatigue life under the same stress level. The fatigue life was accurately predicted using the Smith-Watson-Topper (SWT) method[39]. Zhang et al.[40] evaluated the failure mechanisms of composite-metal SLJ and compared their fatigue performance to composite-composite and metal-metal SLJs, focusing on the influence of substrate material under dynamic loading. However, the study did not account for the geometric parameters of the joints. Zou et al.[41] investigated how the stacking sequence of composite substrates affects the fatigue performance of CFRP-aluminum SLJ.

This study aimed to evaluate the performance of bonded SLJ in CFRP-to-CFRP, Al-to-Al, and CFRP-to-Al configurations, focusing on how CFRP and aluminum adherends affect tensile properties. Specimens were

prepared using 800-grit sandpaper, and surface properties such as contact angle, morphology, roughness, and fracture surfaces were analyzed to assess their effect on SLJ strength.

2. Materials and Methods

2.1. Materials and specimens fabrication

The CFRP composite adherends were fabricated using vinyl ester resin as the matrix and unidirectional carbon fiber as the reinforcement. The adhesive material used in this study is epoxy adhesive. Vacuum-Assisted Resin Infusion (VARI) was employed, utilizing 300 gsm unidirectional carbon fiber and low-viscosity vinyl ester polymer as can be seen in Figure 1. The resin mixture included 1% Percumyl-H (cumene hydroperoxide) as a hardener and 0.3% P-EX (cobalt) as a promoter by mass. To achieve a uniform mixture, the resin, cobalt, and hardener were thoroughly blended before infusion. Each composite panel consisted of 12 layers of unidirectional carbon fabric. Panels were cut to ASTM D5868 dimensions using a waterjet cutting machine, resulting in substrates measuring 101.6 mm × 25.4 mm × 3.3 mm, with each pair forming a single test specimen of CFRP-to-CFRP joint.

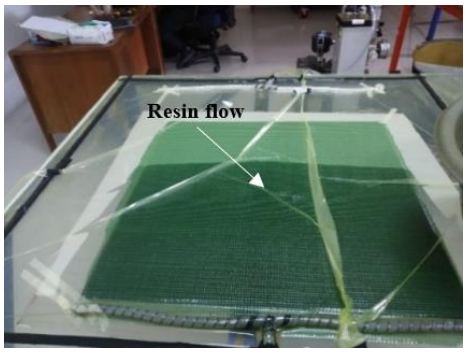

Fig. 1: VARI process.

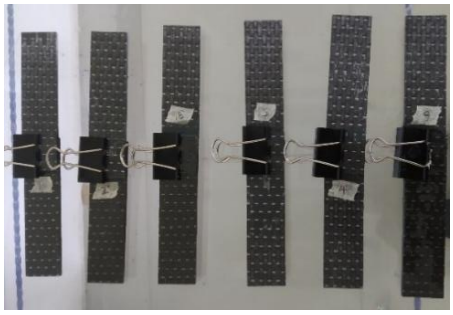

(a)

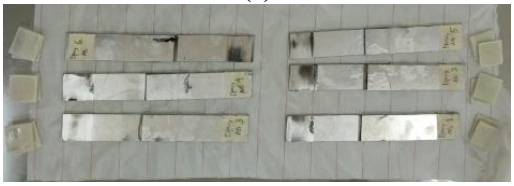

(b)

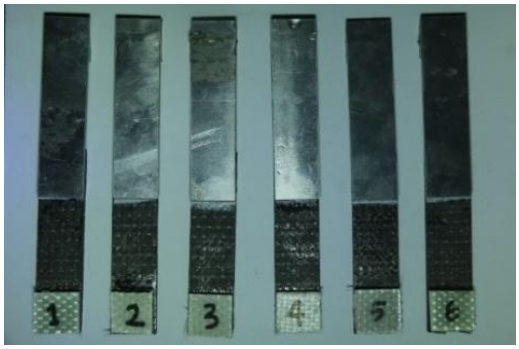

(c)

Fig. 2: SLJ specimens of CFRP-to-CFRP (a), Al-to-Al (b), and CFRP-to-Al (c) configuration.

Aluminum 5052 was utilized as the adherend for Al-to-Al and CFRP-to-Al joints. The aluminum plates were precision-cut to ASTM D5868 dimensions using a waterjet cutting machine. Each pair of aluminum adherends was assembled into a single Al-to-Al joint specimen, while one aluminum adherend paired with a CFRP adherend formed a single CFRP-to-Al connection specimen.

The specimen tabs were fabricated from an 18-layer glass fiber/epoxy composite and cut to dimensions of 25.4 mm × 25.4 mm using the same procedure as the composite adherends. Each specimen was equipped with two tabs, one at each end. Materials such as vinyl ester resin, epoxy, and glass fiber were sourced from Justus Kimia Raya, Indonesia, while unidirectional carbon fiber was obtained from Mitra Composites, and the composites were manufactured at the Research Center for Aeronautics Technology.

Each adherend's 25.4 mm x 25.4 mm bonding area and tab area were sanded using 800-grit sandpaper on a Rockwell sanding machine. The specimens were prepared by bonding two adherends with a 25.4 mm overlap using epoxy adhesive, clamping the overlap with paper clips, and removing excess adhesive. In this study, no adhesive fillet or spew was intentionally included, nor was the fillet geometry controlled during specimen preparation. The specimens were manufactured without applying additional adhesive at the overlap edges, and therefore any minor adhesive overflow that occurred was not considered part of a designed fillet. After curing at room temperature for 24 hours, six SLJ specimens were fabricated for CFRP-to-CFRP (Figure 2a), Al-to-Al (Figure 2b), and CFRP-to-Al (Figure 2c) configurations. The same procedure was applied to attach the tabs to both ends of each specimen.

2.2. Surface roughness, morphology, and contact angle analysis

Surface roughness was measured on adherend surfaces using a Mitutoyo SJ-301 surface roughness tester to determine the arithmetic mean roughness (Ra). The analysis was performed at LTMEPPO, BRIN, Indonesia. Atomic force microscopy (AFM) is an effective method

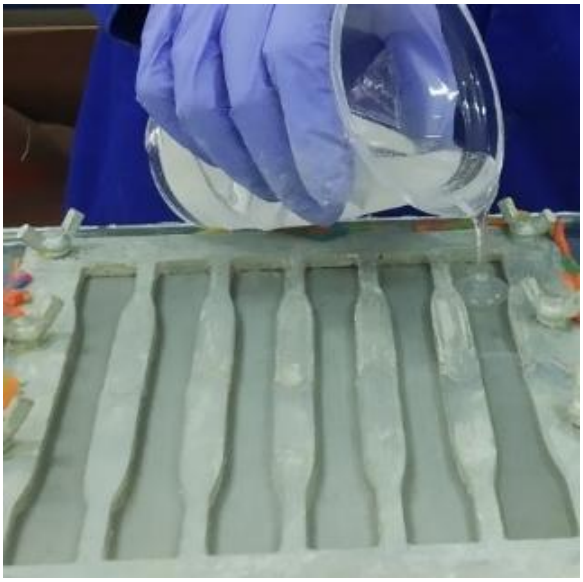

Fig. 3: Preparation of dog bone specimen.

for examining the surface morphology of polymeric composites, providing 3D images with nanometer-scale resolution[42]. AFM observation was performed on adherend surfaces using the Park NX10. This analysis generated detailed 3D topographic images to evaluate surface characteristics.

The liquid contact angle test evaluated wettability, hydrophobicity, and hydrophilicity of adherend surfaces to assess liquid absorption. Testing was conducted using an OCA 25 machine at UPT Laboratory, Diponegoro University for CFRP, and Advanced Physics Laboratory for aluminum.

2.3. Tensile test of adhesives

Tensile tests were conducted on the epoxy adhesive with a 2:1 resin-to-hardener ratio to assess its tensile properties. Five dog-bone-shaped specimens (Figure 3), following ASTM D638 standards, were tested using a 100 kN universal testing machine. The adhesive will be used for SLJ test specimens.

2.4. Single lap shear joint test (SLJ)

The SLJ test was conducted to assess the strength of CFRP-to-CFRP, Al-to-Al, and CFRP-to-Al joints. Tests were performed at the Aeronautics Laboratory - BRIN, using a 100 kN UTM with a 13 mm/min crosshead speed (ASTM D5868). Specimens were installed on the UTM, clamped at both ends (Figure 4), and tested until failure. Six specimens were tested for each configuration.

Load and displacement were recorded by the UTM throughout the test until specimen failure. The applied load was measured by the load cell integrated into the machine, while displacement was obtained from the grip movement. The stress was calculated by dividing the measured load by the overlap area of the joint, and the strain was determined by normalizing the grip displacement to the gage length. All values were automatically recorded by the UTM

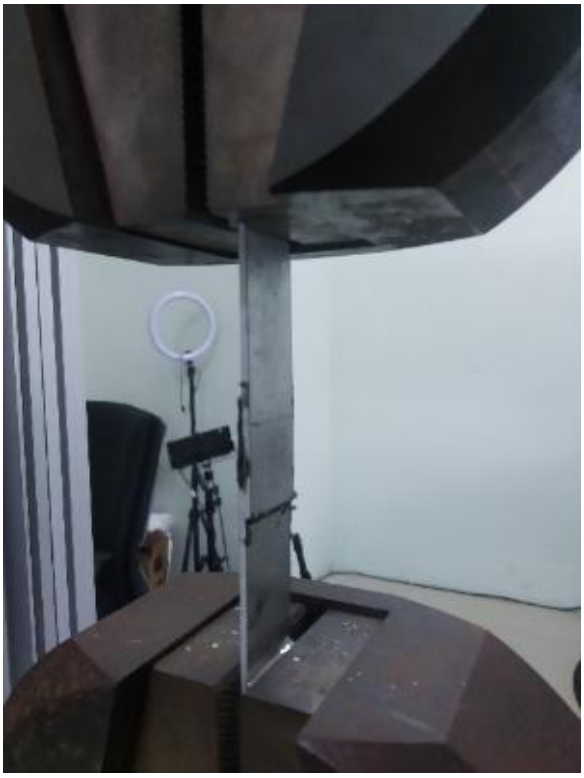

Fig. 4: Single lap joint test.

software, with the overlap dimensions and gage length specified prior to testing.

2.5. Failure analysis

Macro photographs and digital microscopy were employed to examine the joint fracture surfaces. Observations focused on the regions where failure modes occurred on the CFRP-to-CFRP, Al-to-Al, and CFRP-to-Al specimens. Specific failure areas were further analyzed to enhance the visibility of the failure modes.

2.6. Finite Element Analysis (FEA)

FEA is a widely utilized numerical method for simulating and evaluating the behavior of adhesive bonding in various applications. It offers critical insights into the stress distribution within bonded joints, helping engineers ensure the reliability of these connections in real-world scenarios. Several modeling techniques are available in FEA for adhesive bonding, including spring elements, shell elements, and Cohesive Zone Modeling (CZM). Each method provides distinct advantages in capturing the behavior of adhesive bonds under various loading conditions. This research highlights the utility of spring elements for obtaining a fundamental understanding of stress concentration and distribution within adhesive joints. Despite its simplicity, this method can provide valuable insights when combined with experimental validation, paving the way for more refined and advanced adhesive joint designs.

Spring elements offer a simplified method for modeling adhesive bonds, making them especially advantageous

during the initial design stages or when analyzing straightforward joint configurations. This modeling approach was first introduced by Tahmasebi[43] and has since been utilized by Abdurohman et al.[44], who employed plane stress analysis, and by Suwannao et al.[46], who applied plane strain analysis to model 2D adhesively bonded lap joints. These studies demonstrate the versatility of spring elements in providing a fundamental understanding of adhesive joint behavior under varying conditions.

The single lap joint was modeled by shell element for the substrate, spring element for the adhesive layer, and rigid body element. Two springs were positioned in a grid located at the midpoint between the substrates, aligned with the x and y directions. The z-direction was excluded from consideration in this study, as the focus was specifically on the shear stress distribution within the adhesive layer. To ensure proper interaction between the springs and the substrates, a rigid body element was introduced to connect the to the corner node of the shell element representing the substrates.

The spring stiffness values in the x and y directions were derived from the epoxy adhesive stress-strain curve. When an axial force is applied to the single lap joint model, it generates forces within the springs representing the bonded joint. These forces are then used to compute the shear stress distribution within the adhesive layer, providing detailed insight into the adhesive joint's behavior under load. The single lap joint model can be seen in Figure 5.

The stiffness value is required for determining shear stress in the x and y direction.

$$k = \frac{A_a\, G}{t_a} \qquad (1)$$

Where in Eq. 1 k is the stiffness value for the spring element in the x and y direction, A_a is the adhesive element area, E is the elastic modulus of adhesive, G is the shear modulus of adhesive, t_a is adhesive thickness, and v is poisson's ratio.

The adhesive's shear stress can be determined by using spring forces in the x and y direction.

$$\tau_i = \frac{\sqrt{{f_{x,i}}^2 + {f_{y,i}}^2}}{A_a} \qquad (2)$$

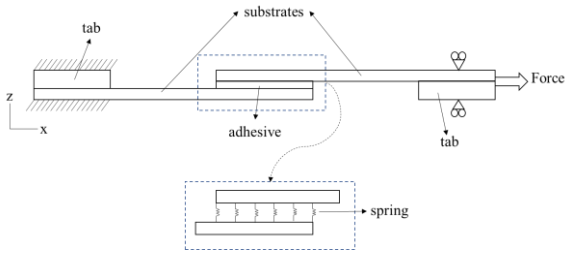

Fig. 5: Single lap joint model.

Where in Eq. 2, τ_i is shear stress at element i, A_a is the adhesive element area, $f_{x,i}$ is spring force in the x-direction at element i, and $f_{y,i}$ is spring force in the y-direction at element i.

3. Results and Discussion

3.1. Surface roughness, surface morphology, and liquid contact angle

The surface roughness (Ra) results are summarized in Table 1. The initial Ra of the CFRP test specimen was 6.48 ± 0.24 µm, indicating a rough surface resulting from the fabrication of unidirectional carbon fiber-reinforced composites. After sanding with 800-grit sandpaper, the Ra was significantly reduced to 1.49 ± 0.19 µm. Untreated specimens exhibited the highest Ra (6.48 ± 0.24 µm), while those treated with 800-grit sanding achieved the lowest Ra (1.49 ± 0.19 µm). These findings confirm that

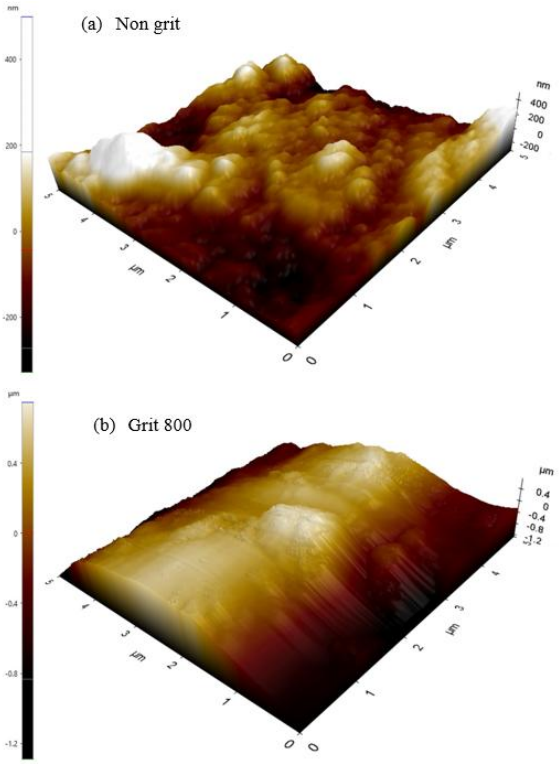

Fig. 6: Surface morphology of the CFRP specimen.

Table 1: Surface roughness (Ra) for CFRP.

Grit size	Ra (µm)
None	6.48 ± 0.24
800	1.49 ± 0.19

Table 2: Liquid contact angle for CFRP.

Grit size	Θ (°)
None	125.3 ± 1.6
800	110.7 ± 0.9

Cite: K. Abdurohman et al., "Experimental Study of Adhesively Bonded Single Lap Joint Behaviour in CFRP-to-CFRP, Al-to-Al, and CFRP-to-Al Configurations". Evergreen, 12 (03) 1531-1544 (2025). https://doi.org/10.5109/7388847.

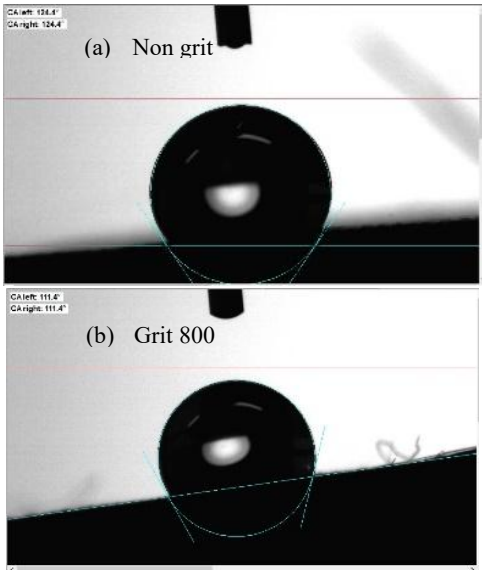

Fig. 7: Liquid contact angle of the CFRP specimen.

sanding effectively reduces surface roughness, improving the surface profile for subsequent bonding applications.

Figure 6 illustrates the surface morphology obtained through atomic force microscopy (AFM). The results demonstrate that sandpaper grit significantly influences the composite's surface morphology and texture. For grit-free specimens, the morphology reflects the composite surface in direct contact with the flat glass mold during manufacturing (Figure 6a). AFM images reveal distinct differences in surface morphology between grit-free and sanded composites. The grit-free surface (Figure 6a) exhibits distributed hill-like peaks, leading to a higher surface roughness value. In contrast, the sanded composite surface (Figure 6b) appears smoother, corresponding to a significantly reduced surface roughness value.

The contact angle measurement results for the CFRP specimens are presented in Figure 7 and Table 2. The untreated specimen surface exhibited a liquid contact angle of 125.3 ± 1.6° (Figure 7a, Table 2), indicating an almost completely hydrophobic surface. These findings align with results reported by Ramaswamy et al.[37]. Following the sanding procedure, the surface contact angle decreased, with CFRP specimens sanded using 800-grit particles showing a reduced contact angle of 110.7 ± 0.9°. This reduction indicates that increasing the surface roughness through sanding leads to a gradual decrease in contact angle, enhancing surface wettability. In summary, the composite surface roughness significantly affects the wettability of the specimen, consistent with findings by Yang et al.[27]. The decrease in contact angle values is likely due to fiber exposure caused by the sanding process[45]. However, despite this decrease, the specimen remains hydrophobic, as indicated by a contact angle exceeding 90°. Figure 7 illustrates liquid droplets resting on the composite specimen's surface. The droplets form obtuse angles with the surface, confirming the hydrophobic nature of the specimen.

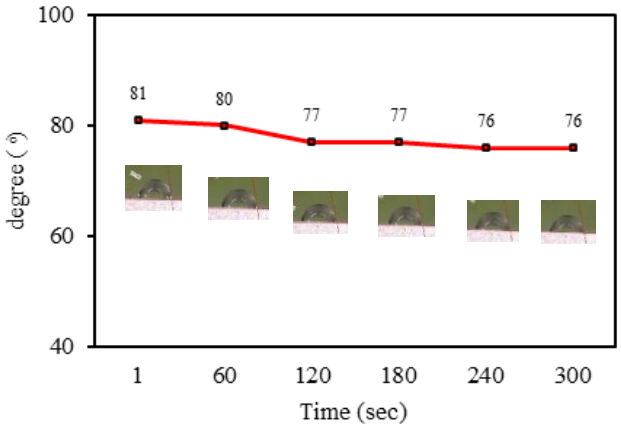

Fig. 8: Liquid contact angle of the Al specimen.

Figure 8 presents the liquid contact angle measurements for aluminum. The results indicate that the initial contact angle of the adherend was 81° at t = 1 second, which gradually decreased to 76° after 300 seconds, suggesting a progressive wetting behavior over time. This value differs from that observed for the CFRP adherend, despite both substrates undergoing the same surface treatment. This indicates that applying the same surface treatment to different materials does not necessarily yield identical results, highlighting the influence of material properties on surface treatment effectiveness.

3.2. Tensile properties of adhesive

Figure 9 illustrates the stress-strain curves of epoxy adhesive for five specimens. All specimens exhibit a consistent trend, characterized by abrupt failure immediately after reaching the ultimate tensile stress, as indicated by the sharp drop in the curves following the peak stress. The stress-strain curves are closely aligned, reflecting the high homogeneity of the specimens and minimal variation in mechanical behavior among them.

The ultimate tensile strength varies slightly between specimens, with the lowest value of 51.88 MPa observed in specimen 1 and the highest value of 57.76 MPa in specimen 3. The average ultimate tensile strength of the epoxy adhesive is 54.30 ± 2.20 MPa, with a tensile modulus of 2.21 ± 0.08 GPa.

These results demonstrate the reliable and uniform mechanical performance of the epoxy adhesive under tensile loading. The small deviation in ultimate tensile strength and modulus further underscores the material's consistency, making it a suitable candidate for applications where predictable tensile behavior is critical.

3.3. Single lap shear joint strength of CFRP-to-CFRP, Al-to-Al, and CFRP-to-Al

Figure 10 presents the stress-strain curves of SLJ specimens with CFRP-to-CFRP adherends. The curves for the six specimens exhibit a similar trend, characterized by two distinct slopes. The first slope is steeper and nearly

Cite: K. Abdurohman et al., "Experimental Study of Adhesively Bonded Single Lap Joint Behaviour in CFRP-to-CFRP, Al-to-Al, and CFRP-to-Al Configurations". Evergreen, 12 (03) 1531-1544 (2025). https://doi.org/10.5109/7388847.

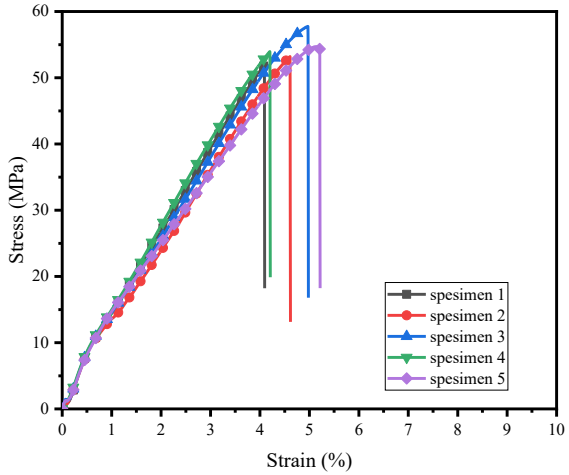

Fig. 9: Stress-strain curves of epoxy adhesive.

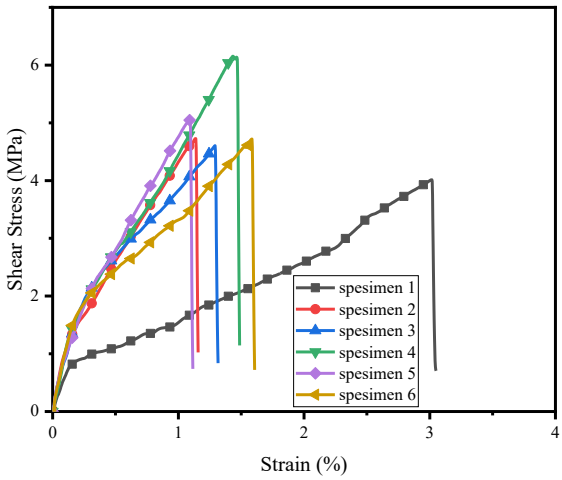

Fig. 10: Stress-strain curves of CFRP-to-CFRP single lap bonded joints.

identical among all specimens, while the second slope is gentler, showing slight variations for specimens 2 to 6. A notable deviation is observed in specimen 1, where the first slope is shorter, and the second slope is significantly gentler compared to the other specimens. Additionally, specimen 1 demonstrates a longer strain at failure, reaching 3%, whereas the strain at failure for specimens 2 to 6 ranges between 1.11% and 1.61%.

Despite these differences, all six specimens exhibit a common behavior after reaching their ultimate shear stress: the curves drop sharply, indicating sudden failure. The lowest shear stress value is recorded at 4.01 MPa for specimen 1, while the highest value is 6.15 MPa for specimen 4. Consequently, the average shear strength of the SLJ CFRP-to-CFRP joints is calculated as 4.88 ± 0.71 MPa. However, if the data from specimen 1 is excluded due to its significantly different slope compared to the other specimens, the average shear strength is calculated as 5.05 ± 0.64 MPa.

This value is comparable to findings from a previous study on SLJ GFRP-to-GFRP bonded joints[44], which utilized the same resin material for the adherends and adhesive but different fiber materials. In that study, the shear strength of SLJ GFRP-to-GFRP joints with the same surface treatment was reported as 4.85 ± 0.24 MPa. This suggests that the resin material used in both the adherends and adhesive predominantly influences the shear strength of adhesive-bonded composite-to-composite joints, while the type of fiber material in the adherends has a negligible or minimal effect. This is likely because the adhesive adherend interface, which is typically dominated by the resin layer, plays a critical role in determining the joint strength.

Figure 11 illustrates the stress-strain curves of SLJ specimens with aluminum-to-aluminum (Al-to-Al) adherends. Similar to the SLJ CFRP-to-CFRP specimens, the curves for SLJ Al-to-Al joints display two distinct slopes. The first slope is steeper, while the second slope is gentler. However, in the case of SLJ Al-to-Al specimens, only specimens 2, 3, and 6 exhibit closely aligned slopes, while specimens 1, 4, and 5 show a wider separation between the two slopes.

The maximum strain values also differ among the specimens, ranging from 0.85% to 2.24%. In terms of shear stress, the smallest maximum value is 2.11 MPa for specimen 5, and the highest value is 3.83 MPa for specimen 2. Based on these values, the average shear strength of SLJ Al-to-Al joints is calculated to be 2.87 ± 0.63 MPa. However, if the data from specimen 1 is excluded due to its notably lower value compared to the other specimens, the average shear strength is calculated as 3.03 ± 0.57 MPa.

When compared to the SLJ CFRP-to-CFRP specimens, which have a shear strength of 5.05 ± 0.64 MPa, the SLJ Al-to-Al joints exhibit a significantly lower strength, approximately 40% of the SLJ CFRP-to-CFRP shear strength. This disparity suggests that the bonding performance of the epoxy adhesive is superior with CFRP adherends compared to aluminum adherends. The enhanced bonding with CFRP can be attributed to the compatibility between the epoxy adhesive and the vinyl ester resin matrix in the CFRP adherends, both of which are polymer-based materials. Conversely, the difference in material composition between the polymer-based adhesive and the metallic aluminum adherend likely contributes to the weaker bond in the SLJ Al-to-Al specimens.

Figure 12 presents the stress-strain curves of SLJ specimens with CFRP-to-Al adherends. The stress-strain behavior of these specimens is highly variable in terms of slope, maximum strain, and maximum shear stress. The lowest maximum strain is 0.18%, observed in specimen 6, while the highest maximum strain is 2.2%, observed in specimen 3. Similarly, the lowest maximum shear stress is 1.28 MPa in specimen 1, and the highest maximum shear stress is 4.33 MPa in specimen 4.

The average shear strength of the CFRP-to-Al SLJ specimens is 2.83 ± 1.22 MPa. However, if the data from specimens 1 and 6 are excluded due to their significantly

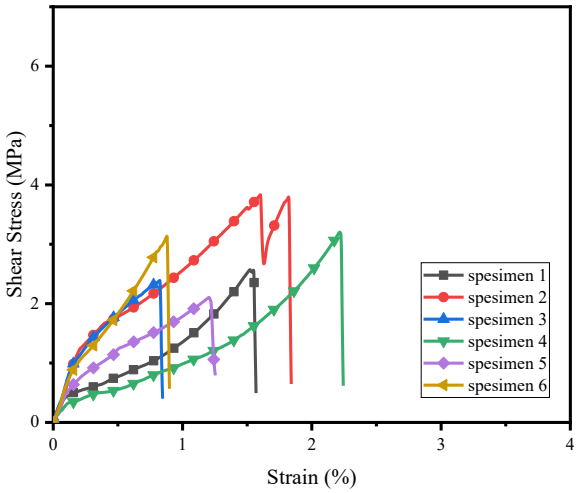

Fig. 11: Stress-strain curves of Al-to-Al single lap bonded joints.

lower values compared to the other specimens, the average shear strength is determined to be 3.52 ± 0.75 MPa. This value is comparable to the shear strength of the SLJ Al-to-Al specimens (3.03 ± 0.57 MPa). This finding indicates that the shear strength of CFRP-to-Al joints is primarily influenced by the bonding performance at the adhesive-aluminum interface. The similarity in shear strength values between CFRP-to-Al and Al-to-Al joints further underscores the dominant role of the aluminum interface in determining bond strength.

A key finding from the mechanical test results is the noticeable variation in peak load and stiffness within specimens belonging to the same group. Such variability is frequently observed in adhesive-bonded joints, as bond quality is influenced not only by curing behavior, adhesive thickness, and intrinsic material properties, but also by the operator's handling during adhesive preparation and application[46]. Due to the high viscosity of the adhesive, mixing is typically performed manually rather than using a controlled mechanical process, which inevitably

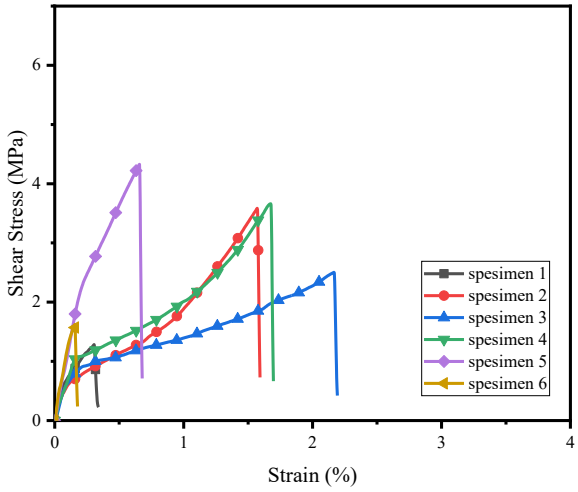

Fig. 12: Stress-strain curves of CFRP-to-Al single lap bonded joints.

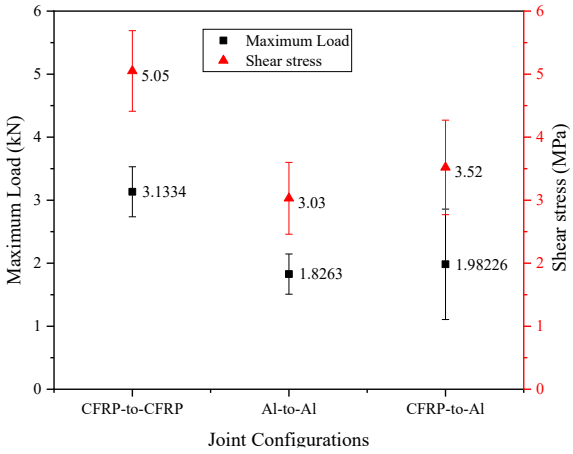

Fig. 13: Maximum load and shear strength value of SLJ specimen.

introduces inconsistencies. Consequently, differences in peak load and stiffness among specimens of the same group are expected, as illustrated in Figure 10, Figure 11, and Figure 12. It should also be noted that increasing the number of tested specimens would improve the reliability of the statistical evaluation of scatter, although it would not eliminate the inherent variability[46].

However, the CFRP-to-Al specimens exhibit the highest standard deviation among all tested configurations as shown in Figure 13, reflecting greater variability and inhomogeneity in the bonding performance when joining dissimilar materials. This suggests that combining CFRP and aluminum introduces additional complexities, likely due to differences in surface energy, thermal expansion, and mechanical properties between the two materials, which can affect the adhesive bond quality and consistency.

3.4. FEA Result

The shear stress distribution within the adhesive layer of a single lap joint will be simulated using the FEA. In this study, the FEA simulation employs a linear static analysis approach. The elastic modulus of the adhesive used in the simulation is based on the average value obtained from tensile tests on epoxy material. According to these tests, the elastic modulus of the epoxy utilized in the simulation is 2.21 GPa. Figure 14 showed the FE model of single lap joint specimen.

The applied loads in the simulation will be based on the tensile test results of single-lap joint specimens. From

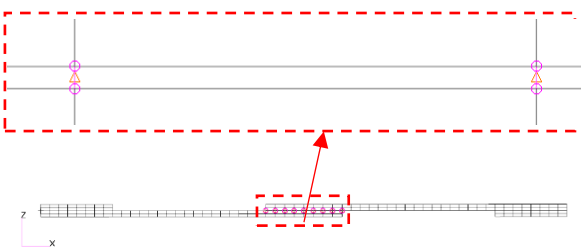

Fig. 14: FE model of single lap joint.

Cite: K. Abdurohman et al., "Experimental Study of Adhesively Bonded Single Lap Joint Behaviour in CFRP-to-CFRP, Al-to-Al, and CFRP-to-Al Configurations". Evergreen, 12 (03) 1531-1544 (2025). https://doi.org/10.5109/7388847.

these tests, it was observed that the maximum load value is highest in the single lap joint with CFRP-to-CFRP material configuration, followed by the CFRP-to-aluminum configuration, and lastly the aluminum-to-aluminum configuration, with respective values of 3133.4 N, 1826.3 N, and 1982.6 N as shown in Figure13.

Figure 15 illustrates a comparison of the shear stress distribution for CFRP-to-CFRP, Al-to-Al, and CFRP-to-Al configurations. This shear stress distribution reflects the shear strength of the single lap joint specimens. All three configurations exhibit a similar trend in the shear stress distribution curve but differ in magnitude. The shear stress distribution reaches its maximum value at both ends of the adhesive layer and gradually decreases to a minimum value at the midpoint of the overlap region. The maximum stress at the adhesive edges represents stress concentrations within the single lap joint specimens, where adhesive failure typically initiates. For the CFRP-to-CFRP configuration, the maximum and minimum shear stress values are 7.63 MPa and 3.53 MPa, respectively. For the Al-to-Al configuration, the maximum and minimum shear stress values are 4.44 MPa and 2.05 MPa, respectively. For the CFRP-to-Al configuration, the maximum and minimum shear stress values are 4.82 MPa and 2.23 MPa, respectively. From Figure 15, it can be observed that the single lap joint with CFRP-to-CFRP material configuration exhibits the highest shear strength, followed by CFRP-to-Al and Al-to-Al configurations. However, the shear stress distribution for the Al-to-Al and CFRP-to-Al configurations are almost overlapping, indicating that the shear strength of these two configurations is very similar.

The shear stress distribution is more easily analyzed using FEA, whereas experimental testing typically provides only the average shear stress. From the shear stress distribution obtained through FEA, the average shear stress value is calculated and then compared with the average shear stress obtained from experimental testing. The FEA analysis in this study was focused on the overall shear stress distribution and its correlation with the experimental results, without addressing the localized stress concentrations at singular points.

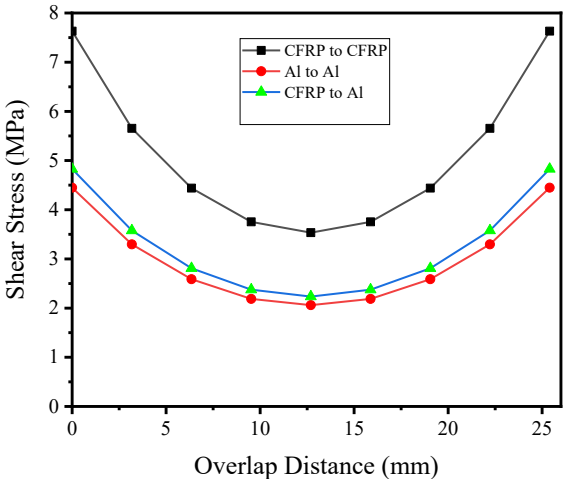

Fig. 15: Shear stress distribution within adhesive layer for CFRP to CFRP, Al to Al, and CFRP to Al.

Table 3: Comparison between FEA and experiment

	CFRP to CFRP	Al to Al	CFRP to Al
τ_ave_FEA (MPa)	5.17	3.01	3.27
τ_ave_exp (MPa)	5.05	3.03	3.52
Difference (%)	2.0	1.0	7.0

From the Table 3, it can be observed that there is a similarity in the shear strength order of the single lap joint between FEA and experimental results. The order of the highest shear strength is CFRP-to-CFRP, followed by CFRP-to-Aluminum, and Aluminum-to-Aluminum for both experimental and FEA results. Regarding the comparison between FEA and experimental results, the Al-to-Al configuration exhibits the smallest discrepancy, followed by the CFRP-to-CFRP configuration, and finally, the CFRP-to-Al configuration. The largest difference is observed in the CFRP-to-Al configuration, primarily due to the less uniform results obtained from the single lap shear specimen testing. This configuration also shows a higher standard deviation, as illustrated in Figure 11, compared to the other two configurations.

3.5. Failure Analysis

Figure 16 illustrates the failure surfaces of SLJ CFRP-to-CFRP specimens after testing. The overall condition of all specimens is shown in Figure 16a, while Figure 16b provides a zoomed-in view of the failure surface in the overlap area. Figure 16c offers a detailed view of the fracture surface on one of the adherends, highlighting the nature of the failure.

The failure mode observed in the SLJ CFRP-to-CFRP specimens is a mix-mode failure, comprising both adhesive and cohesive failures. Cohesive failure is evidenced by the adhesive remnants still attached to the adherend, as seen in Figure 16c. On the other hand, adhesive failure is demonstrated by areas on the adherend surface that lack adhesive, indicating that the adhesive detached entirely from one adherend and transferred to the other.

This combination of adhesive and cohesive failure suggests that the bond quality across the overlap area varies. Some regions exhibit strong bonding between the adhesive and adherend, resulting in cohesive failure, while weaker bonding in other areas leads to adhesive failure. These findings highlight the need for optimizing surface preparation and bonding conditions to enhance the uniformity and strength of adhesive joints in CFRP-to-CFRP configurations.

Cite: K. Abdurohman et al., "Experimental Study of Adhesively Bonded Single Lap Joint Behaviour in CFRP-to-CFRP, Al-to-Al, and CFRP-to-Al Configurations". Evergreen, 12 (03) 1531-1544 (2025). https://doi.org/10.5109/7388847.

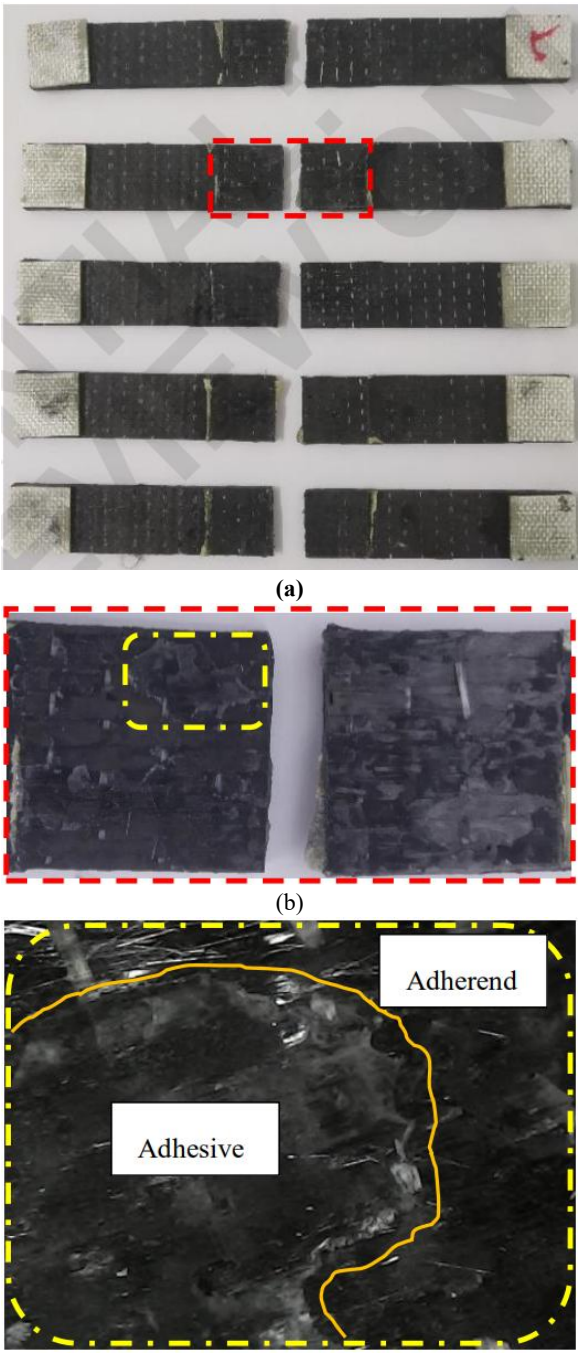

Fig. 16: Photo of CFRP-to-CFRP specimens after the test (a), zoom photo of overlap area (b), and zoom photo of the fracture surface.

Figure 17 presents the failure surfaces of SLJ Al-to-Al specimens after testing. The overall condition of the specimens is depicted in Figure 17a, with Figure 17b providing a zoomed-in view of the overlap area. Figure 17c further zooms into the fracture surface on one adherend, revealing the detailed failure characteristics.

The failure observed in the SLJ Al-to-Al specimens is a mix-mode failure, similar to the failure mode in SLJ CFRP-to-CFRP specimens. Cohesive failure is indicated by the presence of adhesive remnants on the adherend surface, though the layer appears very thin, as seen in

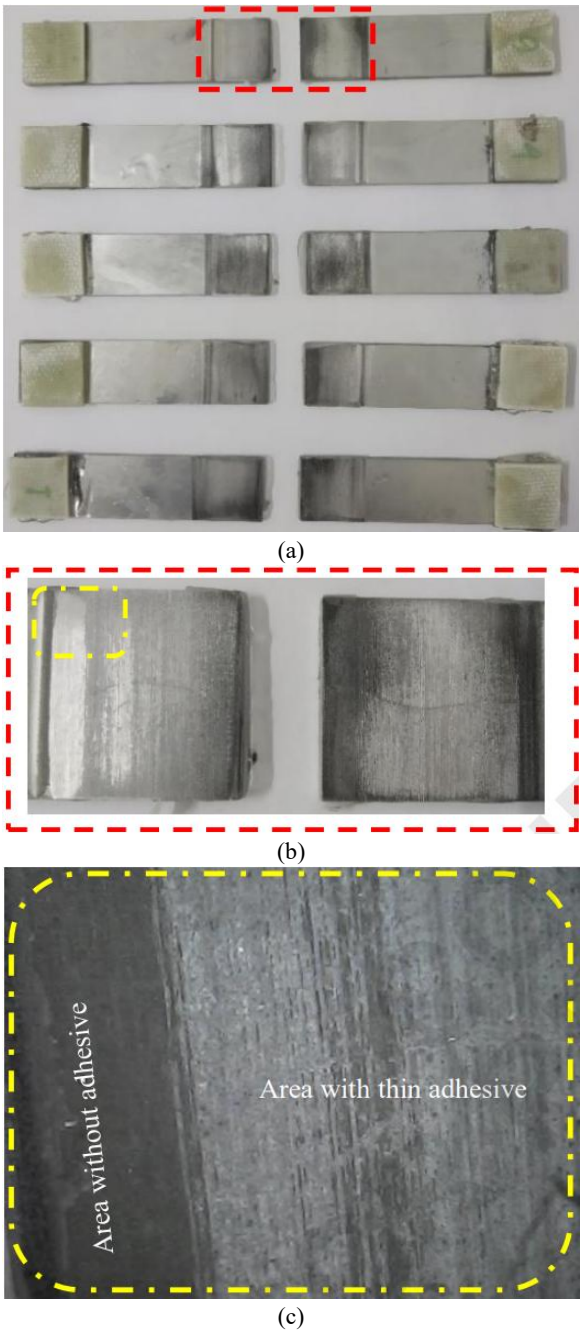

Fig. 17: Photo of Al-to-Al specimens after the test (a), zoom photo of overlap area (b), and zoom photo of the fracture surface.

Figure 17c. Simultaneously, adhesive failure is evidenced by the presence of regions on the adherend surface that lack adhesive entirely.

Despite this similarity in failure mode, the difference in base materials between the adherend (metal) and the adhesive (polymer) results in weaker bonding compared to polymer-polymer systems like SLJ CFRP-to-CFRP. This weaker interfacial bonding is attributed to the material mismatch, as polymers generally form better bonds with composite adherends that share a similar chemical composition. Consequently, the mechanical strength of SLJ Al-to-Al joints is lower than that of SLJ CFRP-to-

Cite: K. Abdurohman et al., "Experimental Study of Adhesively Bonded Single Lap Joint Behaviour in CFRP-to-CFRP, Al-to-Al, and CFRP-to-Al Configurations". Evergreen, 12 (03) 1531-1544 (2025). https://doi.org/10.5109/7388847.

CFRP joints. These findings highlight the influence of adherend material properties on the bonding performance and failure behavior of adhesive joints.

Figure 18 illustrates the failure surfaces of SLJ CFRP-to-Al specimens after testing. The overall condition of all specimens post-testing is shown in Figure 18a. Figures 18b and 18c provide close-up views of the failure surfaces in the overlap area, highlighting distinct failure modes. Figure 18b reveals the predominant failure mode in four out of five specimens, characterized by adhesive failure.

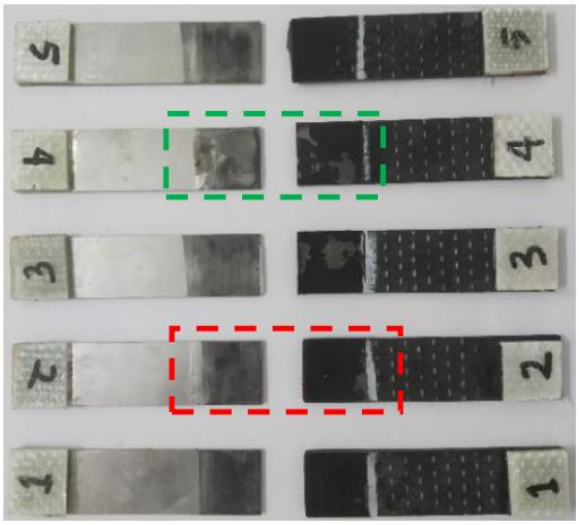

(a)

(b)

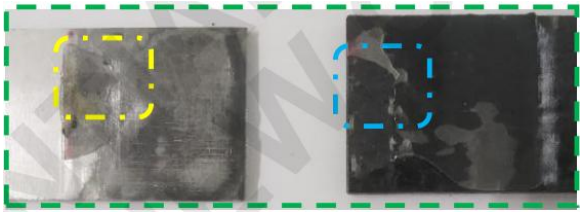

(c)

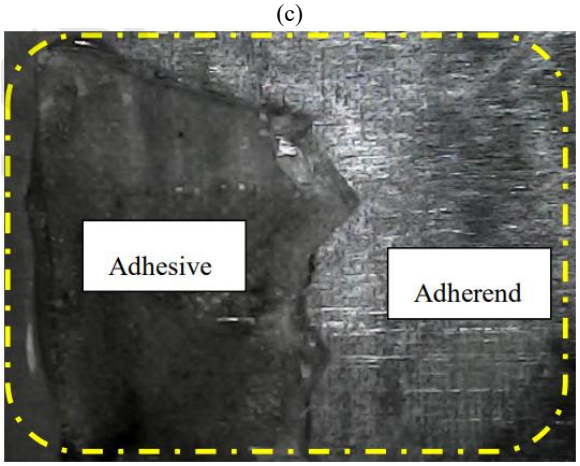

(d)

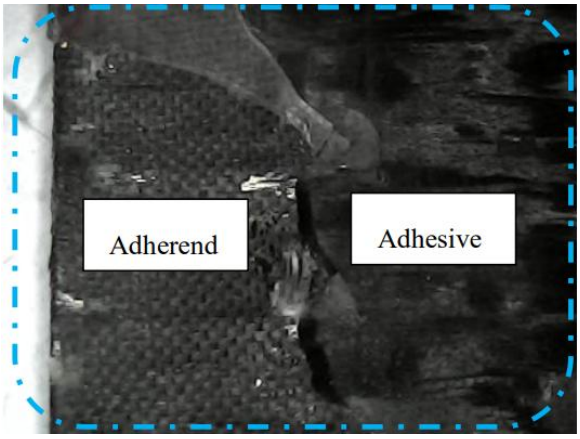

(e)

Fig. 18: Photo of CFRP-to-Al specimens after the test (a), zoom photo of overlap area (b and c), and zoom photo of the fracture surface on Al adherend (d) and CFRP adherend (e).

This mode is evident from the complete detachment of the adhesive layer from the aluminum adherend, leaving the aluminum surface entirely clean while the adhesive remains fully attached to the CFRP adherend. This observation reinforces the superior bonding performance between polymer-based adhesives and CFRP adherends compared to aluminum adherends.

Conversely, Figure 18c highlights a unique failure mode observed in one specimen, where a mix-mode failure (a combination of adhesive and cohesive failure) is evident. The adhesive partially breaks within itself (cohesive failure), as shown by adhesive remnants on one adherend, while other areas experience adhesive detachment (adhesive failure). The detailed surfaces of this mix-mode failure are captured in Figures 18d and 18e, showing the aluminum and CFRP adherends, respectively.

The occurrence of adhesive failure in most specimens underscores the weaker interfacial bonding between the adhesive and aluminum adherend, likely due to the inherent material mismatch between the polymer adhesive and the metallic adherend. In contrast, the single mix-mode failure demonstrates localized areas of stronger bonding, potentially caused by variations in adhesive application or surface preparation. These findings emphasize the critical role of material compatibility and surface treatment in determining the failure behavior of hybrid adhesive joints.

4. Conclusions

This study comprehensively investigated the performance of SLJ in CFRP-to-CFRP, Al-to-Al, and CFRP-to-Al configurations, focusing on the effects of surface preparation and material characteristics on joint strength. The findings underscore the critical role of surface roughness, wettability, and material compatibility in determining the adhesive bond quality and mechanical performance of SLJs.

The CFRP-to-CFRP joints exhibited the highest average

shear strength (5.05 ± 0.64 MPa), attributed to the compatibility between the epoxy adhesive and the vinyl ester resin matrix, as well as effective surface preparation through sanding. Conversely, Al-to-Al joints demonstrated significantly lower shear strength (3.03 ± 0.57 MPa), primarily due to the disparity in material properties between the metallic adherends and polymer-based adhesive. The CFRP-to-Al joints displayed an average shear strength (3.52 ± 0.75 MPa) comparable to Al-to-Al joints but with greater variability, reflecting the complexities introduced by bonding dissimilar materials.

Failure analysis revealed that all configurations predominantly exhibited mixed-mode failures, combining adhesive and cohesive failure mechanisms. The CFRP-to-CFRP joints demonstrated relatively uniform failure patterns, while Al-to-Al and CFRP-to-Al joints showed more pronounced adhesive failure, underscoring the challenges in achieving robust bonding with aluminum adherends.

These results highlight the importance of optimizing surface preparation and adhesive selection to improve joint strength and consistency, especially for dissimilar material combinations. The study provides valuable insights into the design and application of bonded joints in structural engineering, particularly in scenarios involving polymer composites and metals. Future work should explore advanced surface treatments, hybrid adhesives, and environmental aging effects to further enhance joint performance and durability in practical applications.

Acknowledgments

The authors acknowledge the research funding support from “Organisasi Riset Penerbangan dan Antariksa”, No. 27/III.1/HK/2024 by the National Research and Innovation Agency - BRIN, the Republic of Indonesia.

References

1) M.K. Gupta, V. Singhal, and N.S. Rajput, “Applications and challenges of carbon-fibres reinforced composites: a review,” Evergreen, 9 (3) 682–693 (2022). doi:10.5109/4843099.
2) S.W. Park, and D.G. Lee, “Adhesion characteristics of carbon black embedded glass/epoxy composite,” J. Adhes. Sci. Technol., 24 (4) 755–773 (2010). doi:10.1163/016942409X12579497420807.
3) N.K. Yadav, N.S. Rajput, S. Kulshreshtha, and M.K. Gupta, “Investigation of the mechanical and wear properties of epoxy resin composite (ercs) made with nano particle tio2 and cotton fiber reinforcement,” Evergreen, 10 (1) 63–77 (2023). doi:10.5109/6781041.
4) S. Bindu, M.P. Kumar, and K.M. Vinay, “Development and mechanical properties evaluation of basalt-glass hybrid composites,” Evergreen, 10 (03) 1341–1348 (2023).
5) D. Choudhari, and V. Kakhandki, “Characterization and analysis of mechanical properties of short carbon fiber reinforced polyamide66 composites,” Evergreen, 8 (4) 768–776 (2021). doi:10.5109/4742120.
6) D.S. Patil, and M.M. Bhoomkar, “Investigation on mechanical behaviour of fiber-reinforced advanced polymer composite materials,” Evergreen, 10 (1) 55–62 (2023). doi:10.5109/6781040.
7) S. Ray, “Effect of control parameters on erosion wear performance of glass-epoxy composites filled with waste marble powder,” Evergreen, 9 (1) 23–31 (2022). doi:10.5109/4774213.
8) M. Awi, and A.S. Abdullah, “A review on mechanical properties and response of fibre metal laminate under impact loading (experiment),” Evergreen, 10 (1) 111–129 (2023). doi:10.5109/6781057.
9) A.J. Kinloch, “Adhesion and Adhesives: Science and Technology,” 1st ed., Cambridge University Press, 1987. doi:10.1007/978-94-015-7764-9.
10) L.F.M. da Silva, A. Öchsner, and R.D. Adams, “Handbook of Adhesion Technology: Second Edition,” 2018. doi:10.1007/978-3-319-55411-2.
11) A. Sharma, H. Chawla, and K. Srinivas, “Prediction of surface roughness of mild steel finished with viscoelastic magnetic abrasive medium,” Evergreen, 10 (2) 1061–1067 (2023). doi:10.5109/6793663.
12) J.K. Kim, and D.G. Lee, “Adhesion characteristics of plasma-surface-treated carbon fiber-epoxy composite with respect to release films used during demolding,” J. Adhes. Sci. Technol., 18 (4) 473–494 (2004). doi:10.1163/156856104323016379.
13) R.J. Zaldivar, H.I. Kim, G.L. Steckel, J.P. Nokes, and D.N. Patel, “The effect of abrasion surface treatment on the bonding behavior of various carbon fiber-reinforced composites,” J. Adhes. Sci. Technol., 26 (10–11) 1573–1590 (2012). doi:10.1163/156856111X618425.
14) A. Bautista, J.P. Casas-Rodriguez, M. Silva, and A. Porras, “A dynamic response analysis of adhesive - bonded single lap joints used in military aircrafts made of glass fiber composite material undercyclic impact loading,” Int. J. Adhes. Adhes., 102 (April) 102644 (2020). doi:10.1016/j.ijadhadh.2020.102644.
15) H. Purnomo, M.J. Rifa’i, P. Purwoko, D.N. Vicarneltor, M. Ibadi, M.H. Setianto, M. Yudanto, and A.G. Rizkyta, “Implementing surface treatment and adhesive variations for bonded joints between composite gfrp and aluminum at 200 °c,” Eastern-European J. Enterp. Technol., 1 (1 (127)) 60–66 (2024). doi:10.15587/1729-4061.2024.297904.
16) J. Zhang, X. Cheng, X. Guo, J. Bao, and W. Huang,

"Effect of environment conditions on adhesive properties and material selection in composite bonded joints," Int. J. Adhes. Adhes., 96 (December 2018) 1–7 (2020). doi:10.1016/j.ijadhadh.2018.12.001.

17) W. Huang, L. Sun, Y. Liu, Y. Chu, and J. Wang, "Effects of low-energy impact at different temperatures on residual properties of adhesively bonded single-lap joints with composites substrates," Compos. Struct., 267 (February) 113860 (2021). doi:10.1016/j.compstruct.2021.113860.
18) M. Roy Choudhury, and K. Debnath, "Experimental analysis of tensile and compressive failure load in single-lap adhesive joint of green composites," Int. J. Adhes. Adhes., 99 (November 2019) (2020). doi:10.1016/j.ijadhadh.2020.102557.
19) C. Hu, G. Huang, and C. Li, "Experimental and numerical study of low-velocity impact and tensile after impact for cfrp laminates single-lap joints adhesively bonded structure," Materials (Basel)., 14 (4) 1–24 (2021). doi:10.3390/ma14041016.
20) S.T. De Freitas, and J. Sinke, "Failure analysis of adhesively-bonded skin-to-stiffener joints : metal – metal vs . composite – metal," Eng. Fail. Anal., 56 2–13 (2015). doi:http://dx.doi.org/10.1016/j.engfailanal.2015.05.023.
21) I.A. Akpinar, K. Gültekin, S. Akpinar, H. Akbulut, and A. Ozel, "Research on strength of nanocomposite adhesively bonded composite joints," Compos. Part B Eng., 126 143–152 (2017). doi:10.1016/j.compositesb.2017.06.016.
22) C. Sun, P. Jia, C. Chen, A. Moradi, J. Zhou, M. Al Teneiji, W.J. Cantwell, and Z.W. Guan, "The effect of carbon fibre stitching on the tensile behaviour of secondary bonded single- and double-lap composite joints," Compos. Struct., 265 (December 2020) 113774 (2021). doi:10.1016/j.compstruct.2021.113774.
23) S. Sugiman, P.D. Setyawan, S. Salman, and H. Ahmad, "Experimental and numerical investigation of the residual strength of steel-composites bonded joints: effect of media and aging condition," Compos. Part B Eng., 173 (May) (2019). doi:10.1016/j.compositesb.2019.106977.
24) R.C. Dehaghani, D. Cronin, and J. Montesano, "Performance and failure assessment of adhesively bonded non-crimp fabric carbon fiber/epoxy composite single lap joints," Int. J. Adhes. Adhes., 105 102776 (2021). doi:10.1016/j.ijadhadh.2020.102776.
25) R. Tao, M. Alfano, and G. Lubineau, "In situ analysis of interfacial damage in adhesively bonded composite joints subjected to various surface pretreatments," Compos. Part A Appl. Sci. Manuf., 116 (June 2018) 216–223 (2019). doi:10.1016/j.compositesa.2018.10.033.
26) L. Sorrentino, W. Polini, C. Bellini, and G. Parodo, "Surface treatment of cfrp: influence on single lap joint performances," Int. J. Adhes. Adhes., 85 (May) 225–233 (2018). doi:10.1016/j.ijadhadh.2018.06.008.
27) G. Yang, T. Yang, W. Yuan, and Y. Du, "The influence of surface treatment on the tensile properties of carbon fiber-reinforced epoxy composites-bonded joints," Compos. Part B Eng., 160 (July 2018) 446–456 (2019). doi:10.1016/j.compositesb.2018.12.095.
28) M.R. Gude, S.G. Prolongo, and A. Ureña, "Adhesive bonding of carbon fibre/epoxy laminates: correlation between surface and mechanical properties," Surf. Coatings Technol., 207 (March 2019) 602–607 (2012). doi:10.1016/j.surfcoat.2012.07.085.
29) K.Y. Rhee, S.G. Lee, N.S. Choi, and S.J. Park, "Treatment of cfrp by iar method and its effect on the fracture behavior of adhesive bonded cfrp/aluminum composites," Mater. Sci. Eng. A, 357 (1–2) 270–276 (2003). doi:10.1016/S0921-5093(03)00207-7.
30) M.S. Islam, L. Tong, and P.J. Falzon, "Influence of metal surface preparation on its surface profile, contact angle, surface energy and adhesion with glass fibre prepreg," Int. J. Adhes. Adhes., 51 32–41 (2014). doi:10.1016/j.ijadhadh.2014.02.006.
31) A. Baldan, "Adhesion phenomena in bonded joints," Int. J. Adhes. Adhes., 38 95–116 (2012). doi:10.1016/j.ijadhadh.2012.04.007.
32) X. Zhan, Y. Li, C. Gao, H. Wang, and Y. Yang, "Effect of infrared laser surface treatment on the microstructure and properties of adhesively cfrp bonded joints," Opt. Laser Technol., 106 398–409 (2018). doi:10.1016/j.optlastec.2018.04.023.
33) Y. Boutar, S. Naïmi, S. Mezlini, and M.B.S. Ali, "Effect of surface treatment on the shear strength of aluminium adhesive single-lap joints for automotive applications," Int. J. Adhes. Adhes., 67 38–43 (2016). doi:10.1016/j.ijadhadh.2015.12.023.
34) K. Ramaswamy, R.M. O'Higgins, M.A. McCarthy, and C.T. McCarthy, "Influence of adhesive spew geometry and load eccentricity angle on metal-composite bonded joints tested at quasi-static and dynamic loading rates," Compos. Struct., 279 (February 2021) 114812 (2022). doi:10.1016/j.compstruct.2021.114812.
35) H. Grefe, M.W. Kandula, and K. Dilger, "Influence of the fibre orientation on the lap shear strength and fracture behaviour of adhesively bonded composite metal joints at high strain rates," Int. J. Adhes. Adhes., 97 102486 (2020). doi:10.1016/j.ijadhadh.2019.102486.
36) S. Teixeira de Freitas, M.D. Banea, S. Budhe, and S. de Barros, "Interface adhesion assessment of

composite-to-metal bonded joints under salt spray conditions using peel tests," Compos. Struct., 164 68–75 (2017). doi:10.1016/j.compstruct.2016.12.058.

37) K. Ramaswamy, R.M. O'Higgins, A.K. Kadiyala, M.A. McCarthy, and C.T. McCarthy, "Evaluation of grit-blasting as a pre-treatment for carbon-fibre thermoplastic composite to aluminium bonded joints tested at static and dynamic loading rates," Compos. Part B Eng., 185 (January) 107765 (2020). doi:10.1016/j.compositesb.2020.107765.
38) S. Pitta, V. de la Mora Carles, F. Roure, D. Crespo, and J.I. Rojas, "On the static strength of aluminium and carbon fibre aircraft lap joint repairs," Compos. Struct., 201 (May) 276–290 (2018). doi:10.1016/j.compstruct.2018.06.002.
39) V. Kumar, S. Sharma, and A. Singh, "Impact of joint variables on shear and fatigue behavior of composite-metal single-lap adhesive joint," Eng. Fail. Anal., 168 (September 2024) 109079 (2025). doi:10.1016/j.engfailanal.2024.109079.
40) X. Zhang, Y. Ju, A. Zhu, and T. Zou, "Fatigue behavior of single-lap adhesive joints with similar and dissimilar adherends under cyclic loading: a combined experimental and simulation study," Mater. Today Commun., 37 (2898) 107215 (2023). doi:10.1016/j.mtcomm.2023.107215.
41) T. Zou, Y. Ju, Y. Guan, and J. Fu, "Effect of stacking sequence on fatigue performance of cfrp–al single-lap adhesive joints: experimental study," Polymers (Basel)., 14 (23) (2022). doi:10.3390/polym14235088.
42) M. Raimondo, C. Naddeo, L. Vertuccio, K. Lafdi, A. Sorrentino, and L. Guadagno, "Carbon-based aeronautical epoxy nanocomposites: effectiveness of atomic force microscopy (afm) in investigating the dispersion of different carbonaceous nanoparticles," Polymers (Basel)., 11 (5) (2019). doi:10.3390/polym11050832.
43) F. Tahmasebi, "Automation tools for finite element bonded joints analysis of adhesively bonded joint," in: JSME/ASME Int. Conf. Mater. Process., The Japan Society of Mechanical Engineers, Honolulu, 2002: pp. 322–326.
44) K. Abdurohman, R.A. Pratomo, R. Hidayat, R.A. Ramadhan, T.S. Nurtiasto, R. Ardiansyah, M.G.P.P. P, and F.A. Wandono, "Influence of abrasion treatments on performance of adhesively bonded glass/vinyl ester single lap joints," Evergreen, 11 (02) 806–820 (2024).
45) A. Bechikh, O. Klinkova, Y. Maalej, I. Tawfiq, and R. Nasri, "Effect of dry abrasion treatments on composite surface quality and bonded joints shear strength," Int. J. Adhes. Adhes., 113 (November 2021) 103058 (2022). doi:10.1016/j.ijadhadh.2021.103058.
46) C. Barile, C. Casavola, V. Moramarco, C. Pappalettere, and P.K. Vimalathithan, "Bonding characteristics of single-and joggled-lap cfrp specimens: mechanical and acoustic investigations," Appl. Sci., 10 (5) (2020). doi:10.3390/app10051782.